

## Measurement of the tau lifetime

D. Amidei,<sup>(a)</sup> G. H. Trilling, G. S. Abrams, A. R. Baden,<sup>(b)</sup> J. Boyer, F. Butler,  
G. Gidal, M. K. Gold, G. Goldhaber, L. Golding,<sup>(c)</sup> J. Haggerty,<sup>(d)</sup> D. Herrup, I. Juricic,  
J. A. Kadyk, M. E. Nelson,<sup>(e)</sup> P. C. Rowson,<sup>(f)</sup> H. Schellman,<sup>(a)</sup> W. B. Schmidke, P. D. Sheldon,<sup>(g)</sup>  
C. de la Vaissiere,<sup>(h)</sup> and D. R. Wood

*Lawrence Berkeley Laboratory and Department of Physics, University of California, Berkeley, California 94720*

J. A. Jaros, T. Barklow, A. M. Boyarski, P. Burchat,<sup>(i)</sup> D. L. Burke, J. M. Dorfan,  
G. J. Feldman, L. Gladney,<sup>(j)</sup> G. Hanson, K. Hayes, R. J. Hollebeek,<sup>(j)</sup> W. R. Innes,  
D. Karlen, S. R. Klein, A. J. Lankford, R. R. Larsen, B. W. LeClaire, M. E. Levi,  
N. S. Lockyer,<sup>(j)</sup> V. Lüth, C. Matteuzzi,<sup>(k)</sup> R. A. Ong, M. L. Perl, B. Richter,  
K. Riles, and J. M. Yelton<sup>(l)</sup>

*Stanford Linear Accelerator Center, Stanford University, Stanford, California 94305*

T. Schaad<sup>(m)</sup>

*Department of Physics, Harvard University, Cambridge, Massachusetts 02138*

(Received 16 November 1987)

We have used a high-resolution drift chamber in the Mark II detector at the SLAC storage ring PEP to measure the lifetime of  $\tau$  leptons produced in  $e^+e^-$  annihilations at 29 GeV. Based on the flight-path distribution of 807 three-prong  $\tau$  decays, the lifetime is found to be  $(2.88 \pm 0.16 \pm 0.17) \times 10^{-13}$  sec, in agreement with expectations for  $e-\mu-\tau$  universality.

### I. INTRODUCTION

In the decade since its discovery, the  $\tau$  lepton has been extensively studied and is now considered to be a member of a conventional weak doublet, with its own neutrino, and its own conserved lepton number. This third-generation lepton thus becomes a laboratory for precision tests of the standard model. In this paper, we report our measurement of the  $\tau$  lifetime using data recorded by the Mark II detector at the SLAC  $e^+e^-$  colliding-beam facility PEP.

If the  $\tau$  couples to the weak charged current with the same strength as the other leptons, its decay rate to electrons can be calculated analogously to muon decay:

$$\Gamma(\tau \rightarrow e \nu_e \nu_\tau) = \frac{G_F^2 m_\tau^5}{192 \pi^3},$$

where  $G_F$  is the universal Fermi coupling strength,  $m_\tau$  is the  $\tau$  mass, and the  $\nu_\tau$  mass has been neglected. The effect of a  $\nu_\tau$  mass at the present experimental upper bound is negligible compared to other uncertainties in this analysis.<sup>1</sup> Radiative corrections are also small.<sup>2</sup> The  $\tau$  lifetime is simply related to this width through the electron branching fraction

$$\tau_\tau = \frac{B(\tau \rightarrow e \nu_e \nu_\tau)}{\Gamma(\tau \rightarrow e \nu_e \nu_\tau)}.$$

Using the experimentally determined branching fraction<sup>3</sup>  $(17.9 \pm 0.4)\%$ , and mass<sup>4</sup>  $1784 \pm 3$  MeV/ $c^2$ , and including the small radiative corrections, one predicts

$$\tau_\tau = (2.86 \pm 0.06) \times 10^{-13} \text{ sec.}$$

The magnitude of the uncertainty in this prediction is entirely due to the experimental error of the measured electron branching fraction.

The  $\tau$  lifetime provides an unequivocal test of  $\mu-\tau$  universality. In the standard model, all generations couple equally to the same gauge bosons, and  $e-\mu-\tau$  universality is exact.<sup>5</sup> Deviations from universality can arise from mixing in the neutrino sector, or from other new physics.<sup>6</sup> The most stringent limit on  $e-\mu$  universality comes from the ratio of the  $\pi$  branching fractions to  $e$  and  $\mu$ , which implies that, at the 95% confidence level, the Fermi couplings of these particles to the charged weak current are identical to within 2% (Ref. 7). Recently reported measurements of the  $\tau$  lifetime indicate that the  $\tau$  Fermi coupling must lie within 10% of the same value.<sup>8</sup> The lifetime measurement presented here includes refinements and extensions of earlier Mark II results,<sup>9</sup> and supersedes them.

### II. EXPERIMENTAL PROCEDURE

The  $\tau$  leptons for this analysis are produced in the annihilation of 14.5-GeV electrons and positrons from the PEP storage ring at SLAC. Neglecting small radiative corrections, the  $\tau^+\tau^-$  are produced monochromatically at the beam energy. The  $\tau$  lifetime is determined from measurement of the mean decay length:

$$\langle l \rangle = \gamma \beta c \tau_\tau.$$

To determine the decay length, we use the three-prong decay mode of the  $\tau$  to reconstruct a decay vertex, and measure the displacement of this vertex from the beam

spot. When radiative corrections to the  $\tau$  energy are included, the mean path length corresponding to the predicted  $\tau$  lifetime is  $660 \mu\text{m}$ . Good precision in the measurement thus requires high-resolution charged-particle tracking, a well-measured beam position, and careful consideration of systematic errors.

### A. Apparatus

The full details of the Mark II detector at PEP have been given elsewhere.<sup>10</sup> We review here those aspects of the tracking system that are particularly relevant to this analysis.

Charged-particle tracking in the Mark II is carried out with a combination of two cylindrical drift chambers operating in a solenoidal magnetic field of 2.3 kG, all concentric with the beam line. The main drift chamber (DC)<sup>11</sup> contains 16 equally spaced layers of drift cells at radii between 41 and 145 cm. Six of these layers contain axial sense wires; in the other ten, the sense wires are at  $\pm 3^\circ$  to provide stereo information. The position resolution is approximately  $200 \mu\text{m}$  per layer.

In the space between the beam vacuum pipe and the inner wall of the main drift chamber is a smaller high-resolution device, known as the vertex chamber (VC).<sup>12</sup> This cylindrical chamber, 1.2 m in length and 0.70 m in diameter, operates with seven layers of drift cells strung between 5-cm-thick aluminum end plates. To minimize the error due to multiple Coulomb scattering, the inner shell is made from beryllium, and serves as the beam pipe. Amounting to only 0.6% of a radiation length, it is the only material between the interaction point and the first vertex chamber position measurement.

The wire array is composed of alternating cathode only and cathode/sense layers, all strung parallel to the beam axis. Sense wires are located to  $15 \mu\text{m}$  accuracy with individual nylon feedthroughs. The radial distance between layers, 4.2 mm, and the distance between adjacent wires at the same radius, 5.3 mm, specify a pattern of roughly hexagonal drift cells. Four layers of inner drift cells lie just outside the beam pipe, at radii from 10.1 to 12.6 cm, and another three layers are clustered at radii from 30.4 to 32.0 cm. In all, there are 270 drift cells in the inner layers and 555 drift cells in the outer.

The chamber operates with a 50/50 mixture of argon-ethane, plus 0.4% ethyl alcohol.<sup>13</sup> At our standard discriminator setting of  $200 \mu\text{V}$ , the chamber is fully efficient at 1.950 kV; our operating voltage is somewhat above this, at 2.10 kV. The resolution of the electronics used for the drift time measurement is approximately 250 psec.

### B. Off-line reconstruction and tracking

The first step in off-line data reconstruction is the determination of the geometric placement of the vertex detector relative to the main drift chamber. We use a right-handed coordinate system centered in the DC with positive  $z$  axis parallel to the electron beam. The VC position is characterized in terms of three small Cartesian rotations, and two small displacements in  $x$  and  $y$ ; the constants are found by least-squares minimization of the

tracking  $\chi^2$  in both chambers for a large ensemble of tracks from Bhabha scattering. The resultant geometry is used as a starting point in a separate algorithm to find the space-time relation in the VC, and this two-step process is repeated until it converges.

The electron drift velocity is saturated throughout the VC drift cell. This ensures a space-time relation which is approximately linear over most of the drift region. The constant spacing between sense and field wires at the same radius allows the use of a single such relation for all drift cells. We use the Bhabha track sample to fit the space-time relation to a third-order polynomial, and find significant deviations from linearity only very near and very far from the sense wire. Attempts to use separate relations for those special regions yield no significant improvement in resolution.

To determine track parameters, a least-squares fit to drift times in both vertex and main drift chambers is made. Precise angular and position measurements in the  $x$ - $y$  plane are supplied by the VC, while dip and curvature information is provided by the DC. To take account of geometric uncertainties in the DC and in the relative VC-DC geometry, we allow small VC-DC relative shifts in the  $x$ - $y$  position ( $\sigma = 200 \mu\text{m}$ ) and in azimuth ( $\sigma = 0.3 \text{ mr}$ ) in the fits. In Fig. 1 we show the distribution of  $\chi^2$  constructed from VC residuals on Bhabha tracks with measurements in all seven layers, using an average resolution of  $95 \mu\text{m}$  per layer. Since our fit effectively uses the VC information to determine two parameters ( $x$ - $y$  position and slope), we expect a  $\chi^2$  distribution appropriate to five degrees of freedom. This distribution is also plotted in Fig. 1 and, except for the tails, describes the data well.

The position precision of tracks reconstructed in the VC-DC system has been discussed in detail by Gladney *et al.*<sup>14</sup> From the measured tracking residuals in the vertex detector, and the known scattering contributions, the track-position resolution in the  $x$ - $y$  plane, extrapolated to the beam center, is predicted to be

$$\sigma_0 (\mu\text{m}) = \{(85)^2 + [95/P(\text{GeV}/c)]^2\}^{1/2}.$$

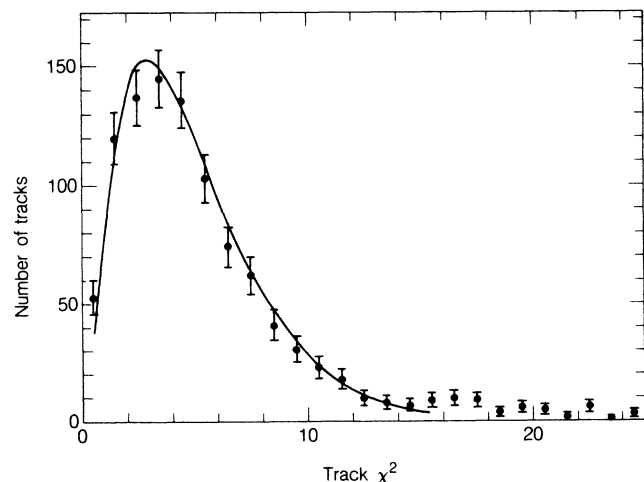


FIG. 1. Vertex detector track  $\chi^2$  for Bhabha-scattering tracks. The fit is the expected form for 5 degrees of freedom.

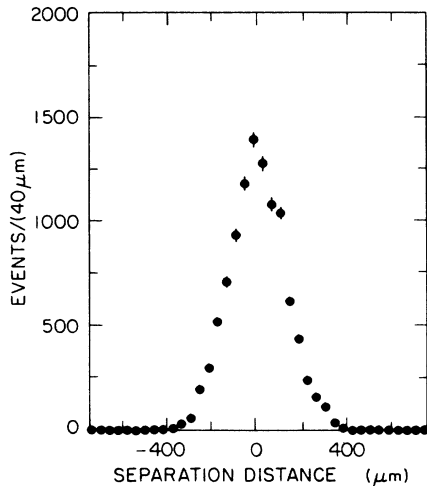


FIG. 2. Extrapolated separation distance between Bhabha tracks at the interaction point.

The first term measures the intrinsic tracking performance, and the second measures the effect of multiple Coulomb scattering. We have verified this prediction with a large sample of Bhabha scattering events. Ignoring multiple Coulomb scattering in this case, we expect the rms separation distance of the two tracks at the origin to be just  $\sqrt{2}$  times the intrinsic resolution there, or  $120 \mu\text{m}$ . The measured distribution of these separation distances, shown in Fig. 2, has a rms width of  $124 \mu\text{m}$ . Additional studies with Bhabha tracks have also demonstrated the absence of any azimuthal dependence of track parameters measured at the beam center.<sup>14</sup>

### C. Beam size and position

The position and shape of the luminous region are necessary ingredients in the determination of the  $\tau$  path length. The beam position is derived from a measurement of the average intersection point of Bhabha tracks whose directions, projected into the  $x$ - $y$  plane, lie within  $100 \text{ mrad}$  of the vertical and horizontal axes. The average beam position measurement is accurate to  $20 \mu\text{m}$  vertically and  $50 \mu\text{m}$  horizontally, and is stable from one storage ring fill to the next. The beam size is derived from the distribution of Bhabha track impact parameters relative to the measured beam center, corrected for the VC resolution. The result from a fraction of our data is<sup>15</sup>

$$\sigma_{bx} = 481 \pm 18 \mu\text{m} \quad \text{and} \quad \sigma_{by} = 62 \pm 9 \mu\text{m} .$$

Further detail on beam position measurement and monitoring can be found in Ref. 14.

## III. SELECTION OF THE $\tau$ SAMPLE

$\tau$  pair production at 29-GeV center-of-mass energy has a distinctive signature and can be isolated with little background. Candidate events are subjected to quality cuts to ensure the reliability of the tracking information. This analysis is based on data recorded at PEP over a period from 1981 to 1984, with an integrated luminosity of  $206 \text{ pb}^{-1}$ .

### A. Event selection

With the exception of a very small branching fraction to five prongs, all  $\tau$  decay modes produce either one or three charged tracks in the final state.<sup>16</sup> Our sample of three-prong decays is selected from events with zero total charge which contain either a pair of three-prong jets in opposite hemispheres or a single track and a three-prong jet in opposite hemispheres. To ensure that the event originates in an  $e^+e^-$  collision we require that the overall event vertex lie within 2 cm of the beam center in the  $x$ - $y$  plane, and within 5 cm along the beam axis.

Further cuts are applied to this sample to minimize anticipated backgrounds. We require that each three-prong candidate have charge  $\pm 1$  and an invariant mass, based on the charged particles, between  $0.7 \text{ GeV}/c^2$  and  $1.5 \text{ GeV}/c^2$ . In addition, we calculate the mass of the  $\tau$ -like system including nearby neutral energy recorded by the liquid-argon calorimeter and require that it be less than  $2.0 \text{ GeV}/c^2$ . In two-jet (six prong) events, failure of either jet results in the exclusion of both.

Tau pairs produced in the two-photon collision process  $e^+e^- \rightarrow e^+e^-\tau^+\tau^-$  are rejected through the requirement that the total charged energy in the event exceed 5.0 GeV, and that the energy of each three prong exceed 3.0 GeV. We suppress these events because their  $\tau$  energies are substantially less than the beam energy, and not well determined.

Finally, we must protect against radiative Bhabha and  $\mu^+\mu^-$  events which can mimic the 3+1 topology if the photon converts to an electron-positron pair. We therefore require that the total charged energy in each event be less than  $0.9E_{c.m.}$ , and that the three-particle invariant mass, calculated assuming that all tracks are electrons, exceed  $300 \text{ MeV}/c^2$ .

### B. Backgrounds

The level of the remaining background in this sample has been studied by Monte Carlo simulation. The Monte Carlo simulation includes accurate representation of VC and DC resolutions, multiple Coulomb scattering in the beam pipe, chamber wires, and VC-DC interface, nuclear scattering and absorption in the beam pipe, pion and kaon decay, photon conversions, and the pattern of inefficient drift cells in the two chambers.

The hadronic event sample is generated using the Feynman-Field fragmentation model and known heavy-quark parameters. The magnitude of hadronic backgrounds satisfying our cuts is estimated to be  $(4.0 \pm 0.9)\%$  of the candidate event sample. As a rough check on the simulation, we have studied real four- and six-prong hadronic events with  $\tau$ -like topologies satisfying the three-pion mass cuts:

$$2 < M(3\pi) < 4 \text{ GeV}/c^2 ,$$

$$2 < M(3\pi + \text{neutrals}) < 4 \text{ GeV}/c^2 .$$

The number of such events satisfying our  $\tau$  selection criteria (except for the  $3\pi$  mass cuts) is found to be 3 in the data and is expected to be 4 from the Monte Carlo simulation. Because of the poor statistics, we assign a 50% uncertainty to the hadronic background, which we take

to be  $(4 \pm 2)\%$ .

Two-photon  $\tau$  production is estimated from a Monte Carlo simulation which generates  $\tau$  pairs from  $2\gamma$  collisions via the double equivalent photon approximation. After applying all of the event and track cuts, we find a background from this source of  $(3.0 \pm 1.0)\%$ .

Both of these background estimates include a correction for the somewhat higher efficiency for track finding in the Monte Carlo relative to real data. Backgrounds from radiative QED processes are found to be negligible and we place an upper limit of 1% on such contributions.

### C. Track quality cuts

The selection outlined in Sec. III A yields 1786 three-prong decay candidates. We apply to this sample a further set of tracking quality cuts to ensure that the decay point is well measured. To guarantee a good curvature determination, we require each track to have six or more measurements in the main drift chamber. To ensure a good extrapolation to the origin, we require at least two measurements in the VC inner layers and at least one in the VC outer layers. To reduce multiple Coulomb scattering and the probability of nuclear scattering, we require that the momentum of each of the three tracks exceed  $400 \text{ MeV}/c^2$ .

We have studied the tracking  $\chi^2$  for the VC information alone, and find that tracks from  $\tau$  events have an average resolution per layer about 15% larger than that inferred from Bhabha-scattering events as discussed in Sec. II B. The cause has been traced to channel-to-channel cross talk which occurs in the electronics when tracks are close together in the chamber.<sup>17</sup> We therefore refit all three-prong tracks with the VC errors increased by 15%. In Fig. 3, we compare the  $\chi^2$  distribution for tracks fit in this manner to the expected form. The sample is limited to tracks with seven VC measurements and, as discussed in Sec. II B, the anticipated curve is for 5 degrees of freedom. Again, there is good agreement, except for the tails, and we conclude that the VC resolution in

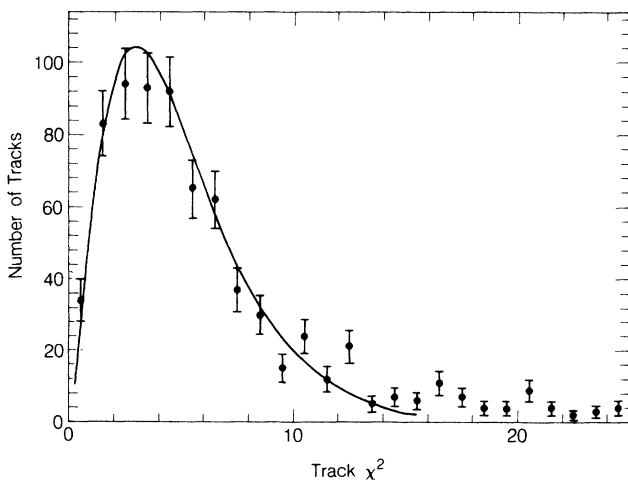


FIG. 3. Vertex detector track  $\chi^2$  for tracks in the  $\tau$  three-prong decays, after rescaling the VC resolution by 15%. The fit is the expected form for five degrees of freedom.

these events is reasonably well understood. For each accepted decay in our sample, we require that all three tracks have a VC  $\chi^2$  less than 5.0 per degree of freedom, and a  $\chi^2$  for the full fit in both chambers of less than 4.0 per degree of freedom. The application of the above cuts reduces the sample to 1296 passing decays.

## IV. DETERMINATION OF THE $\tau$ LIFETIME

### A. Vertex determination

The most probable location of the  $\tau$  decay point in the plane perpendicular to the beam is found by a one-constraint, least-squares fit to the high-precision tracking information in that plane. Measurement and multiple-scattering errors in all of the track parameters are taken into account, and the output of the vertexing calculation includes the  $(x, y)$  coordinates of the best-fit decay point, the corresponding errors, and the  $\chi^2$  of the fit. The distribution of this  $\chi^2$  is shown in Fig. 4. To reduce the probability that one or more of the tracks undergo large scattering in the beam pipe, only those events with vertex  $\chi^2 < 4.0$  are accepted. An additional consistency check is based on the much less accurate  $z$  coordinates of the  $\tau$  secondaries at the best-fit  $(x, y)$  decay point. We define the quantity  $\chi_z^2$ :

$$\chi_z^2 = \sum_{i=1}^3 \frac{(z_i - z_{av})^2}{\sigma_{z_i}^2},$$

where  $z_{av}$  is the mean  $z$  coordinate of the three tracks, and  $\sigma_{z_i}$  the calculated error of the  $z$  coordinate of the  $i$ th track. The distribution of  $\chi_z^2$  is expected to correspond to 2 degrees of freedom. The experimental distribution is somewhat broader, and a rather loose cut at  $\chi_z^2 < 20$  is made. It should be emphasized that the decay point  $(x, y)$  coordinates depend almost exclusively on the vertex chamber measurements, with the less precise main drift chamber providing the curvature information needed for track extrapolations.

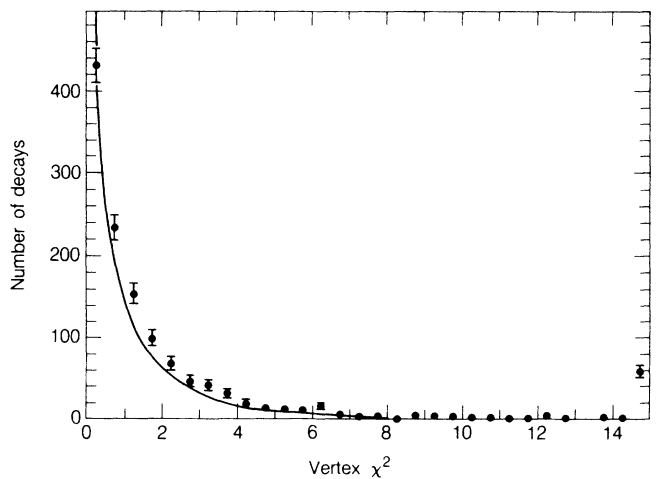


FIG. 4. Vertex  $\chi^2$  distribution for the fit to the three-prong vertex in the  $xy$  plane. The solid line is the expected form for 1 degree of freedom.

### B. The $\tau$ decay length

We now consider, for each event, the optimal estimate of the  $\tau$  decay length. The situation for a typical event is summarized in Fig. 5, which shows a magnified view near the interaction region, and indicates the beam ellipse as well as the decay vertex error ellipse. We have already discussed the beam ellipse, which is taken to have a position and size as described in Sec. II C. The vertex error ellipse is obtained from the vertex calculation discussed in the previous section. We approximate the  $(x, y)$  component of the  $\tau$  direction by the projection of the vector sum of the momenta of the three charged secondaries. This approximation neglects the effect on the  $\tau$  direction of the final-state neutrino and any  $\pi^0$  secondary. The error thereby introduced is small and will be discussed later. Taking this approximate  $\tau$  direction as fixed, we make a one-constraint fit to obtain the best estimates of the production and decay points, and the corresponding decay length. The two-dimensional decay length and its error are given by

$$l' = \frac{x_v \sigma_{yy} t_x + y_v \sigma_{xx} t_y - \sigma_{xy} (x_v t_y + y_v t_x)}{\sigma_{yy} t_x^2 + \sigma_{xx} t_y^2 - 2\sigma_{xy} t_x t_y},$$

$$\sigma'_l = \left[ \frac{\sigma_{xx} \sigma_{yy} - \sigma_{xy}^2}{\sigma_{yy} t_x^2 + \sigma_{xx} t_y^2 - 2\sigma_{xy} t_x t_y} \right]^{1/2},$$

where  $(x_v, y_v)$  are decay vertex positions relative to the center of the beam ellipse,  $(\sigma_{xx}, \sigma_{xy}, \sigma_{yy})$  are error matrix elements obtained by adding vertex and beam position error matrices, and  $(t_x, t_y)$  are the two-dimensional direction cosines of the  $\tau$  line of flight.

The two-dimensional quantities  $l'$  and  $\sigma'_l$  are converted to three dimensional  $l$  and  $\sigma_l$  through division by  $\sin\theta_\tau$ , where  $\theta_\tau$  is the polar angle of the  $3\pi$  momentum direction. The distribution of  $\sigma_l$  is shown in Fig. 6. To ensure a sample with maximal signal-to-noise ratio, we retain only those decays for which  $\sigma_l < 1.4$  mm, and also require that the  $\tau$  production point derived from the above fit be within 2 standard deviations of the measured beam center. Our final sample, which passes all cuts up to this point, contains 807 decays.

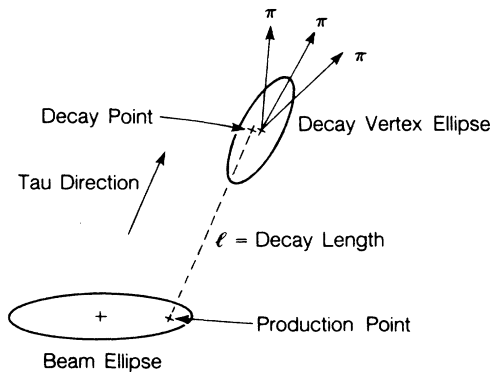


FIG. 5. Schematic view of the  $\tau$  decay vertex, showing beam and decay vertex error ellipses. The decay length, as well as the decay and production points are found by the fit discussed in Sec. IV B.

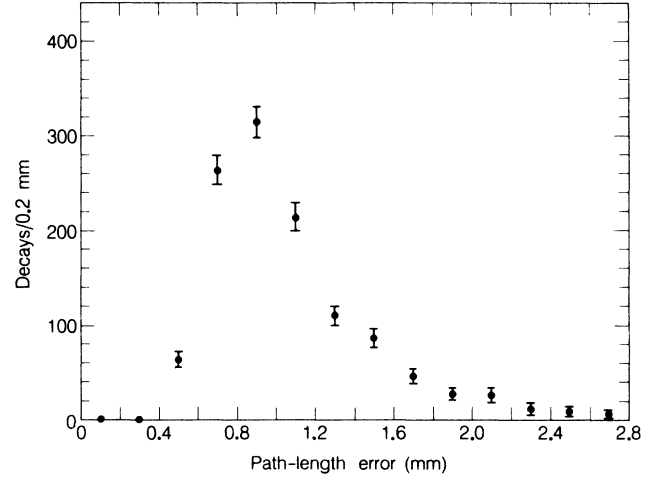


FIG. 6. Distribution of  $\sigma_l$ , the three-dimensional fitted error in decay length, for the final  $\tau$  sample.

### C. Maximum-likelihood analysis

We construct a likelihood function

$$L = \prod_{i=1}^N P_i(l_i, l_\tau),$$

where  $l_\tau$  is the mean  $\tau$  decay length that we wish to determine and  $l_i$  is the measured decay length for the  $i$ th event. The individual event probability  $P_i$  is given by the convolution of the exponential decay distribution with a Gaussian resolution function:

$$P_i(l_i, l_\tau) = \frac{1}{l_\tau} \frac{1}{\sqrt{2\pi\sigma_i^2}} \int_0^\infty \exp(-x/l_\tau) \times \exp[-(x - l_i)^2/2\sigma_i^2] dx,$$

where  $\sigma_i$  is the calculated error in  $l_i$ . The best-fit value of  $l_\tau$  is obtained by maximization of  $L$ .

There is an important subtlety in the application of this procedure to the  $\tau$  decay length data. As seen from Fig. 6, the typical values of  $\sigma_i$  are comparable in magnitude to the anticipated value of  $l_\tau$ . As a consequence of this relation, the result of the likelihood fit is sensitive to the values of  $\sigma_i$ . Indeed, the rms width of the distribution of  $l_i$  is easily shown to be

$$\langle (l_i - l_\tau)^2 \rangle = \sigma_i^2 + l_\tau^2.$$

The width information is used in the likelihood fit, and any underestimate of  $\sigma_i$  will be compensated by an upward bias in the fitted value of  $l_\tau$ . Our calculated values of  $\sigma_i$  are, indeed, likely to be underestimates, since various non-Gaussian tails are not included. To avoid this difficulty, at the cost of slightly increased statistical errors, we include in our fit an additional parameter  $R$ , which scales all of the calculated errors as

$$\sigma_i \rightarrow R \sigma_i.$$

By introducing  $R$  as a free parameter, we effectively base

the determination of  $l_\tau$  on an appropriately weighted mean value of the individual  $l_i$ , rather than on the detailed shape of the  $l_i$  distribution.

#### D. Determination of the $\tau$ lifetime

The distribution of decay lengths for the sample of 807 three-prong decays which pass all of the cuts described in previous sections is shown in Fig. 7. The results of the maximum-likelihood analysis, as applied to this sample, are

$$l_\tau = 635 \pm 35 \mu\text{m} ,$$

$$R = 1.05 \pm 0.04 .$$

The expected distribution parametrized by these values is shown superimposed on Fig. 7, and is seen to provide a satisfactory representation of the data.

Contamination of the  $\tau$  sample with the backgrounds discussed in Sec. III B will tend to reduce the apparent mean decay length. To determine the magnitude of this effect, we combine appropriate amounts of the simulated hadron and two-photon backgrounds with a simulated  $\tau$  sample of nominal lifetime, and study the corresponding change in the measured decay length. An alternative technique uses the Monte Carlo events to estimate the mean decay length of each of the background classes, and then considers the effect of the appropriate fraction of each class on the overall mean. The results of the two techniques are consistent, and imply that the presence of the background lowers the result by  $31 \pm 10 \mu\text{m}$ . Adding this correction to our maximum-likelihood result, we find

$$l_\tau = 666 \pm 37 \mu\text{m} ,$$

where the quoted statistical error has been scaled up by the same fractional amount as the path length. With the appropriate correction for initial-state radiation, the mean  $\tau$  total energy is expected to be 13.9 GeV. We then find a  $\tau$  lifetime:

$$\tau_\tau = (2.88 \pm 0.16) \times 10^{-13} \text{ sec} .$$

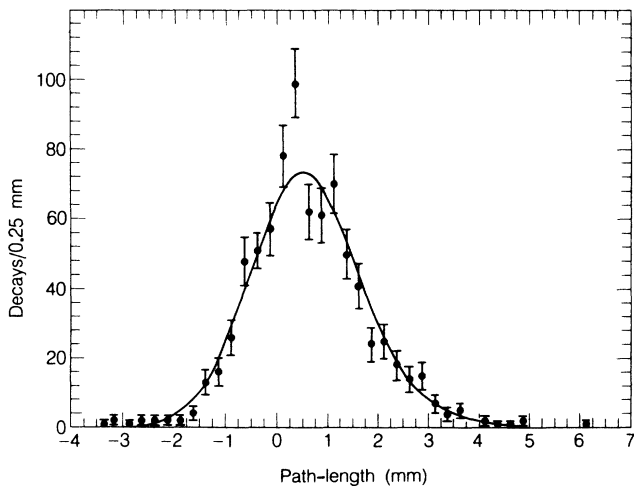


FIG. 7. Distribution of  $l_i$ , the three-dimensional fitted  $\tau$  path length, in the final sample. The solid curve is the result of the fit in Sec. IV D.

The quoted error is statistical; systematic uncertainties are discussed in the next section.

## V. CHECKS ON THE ANALYSIS

### A. Measurement bias

Early measurements of the  $\tau$  lifetime required substantial corrections to the observed decay lengths to remove a bias which arose from a correlation between the measured decay length and its estimated error. Events with fluctuations toward longer measured decay lengths were associated with smaller track extrapolation errors and thus smaller vertex errors, while fluctuations toward shorter decay lengths were assigned correspondingly larger vertex errors. The former events were consequently given greater weight in the likelihood fit, biasing the result toward a longer mean decay length.

The improved tracking resolution and reduced multiple Coulomb scattering of this experiment should reduce such bias to a small level. To confirm this, and to check for the presence of other potential systematic effects, we have studied our analysis technique using Monte Carlo-generated  $\tau$  decays. In addition, to check for effects not reproduced by the Monte Carlo simulation, we have made comparisons between  $\tau$ -like control samples constructed from both real and simulated hadronic events. These studies are discussed below.

### B. Monte Carlo simulation

Two samples of 20 000  $\tau$  decays were created with lifetimes of 0 and  $2.80 \times 10^{-13}$  sec. Each sample is subjected to the complete analysis procedure and maximum-likelihood fit. We note here that in the limit in which the mean decay length is very small compared to  $\sigma_l$ , the formula for  $P_i$  discussed in Sec. IV C poses numerical problems. For the zero lifetime sample, we instead approximate  $P_i$  by the Gaussian

$$P_i(l_i, l_\tau) = \frac{\exp[-(l_i - l_\tau)^2 / 2(\sigma_l^2 + l_\tau^2)]}{[2\pi(\sigma_l^2 + l_\tau^2)]^{1/2}} .$$

This expression has the same mean and the same rms deviation as the exact result.

The fit values for the final samples of about 1500 simulated decays at each lifetime are  $28 \pm 20$  and  $597 \pm 22 \mu\text{m}$ , in good agreement with the mean generated path lengths in these samples of 0 and  $612 \mu\text{m}$ . The fitted value of  $R$  is consistent with unity in each case. Furthermore, in the zero lifetime sample, the distribution of the ratio  $l_i / \sigma_l$  is accurately fit by a Gaussian of unit standard deviation, indicating that, in Monte Carlo events, our analysis does yield a Gaussian error which is well represented by the calculated  $\sigma_l$ .

### C. Hadronic control sample

Having checked the validity of our analysis on a Monte Carlo sample, we need to verify how well the simulation reproduces the experimental environment. For this purpose, we construct, from hadronic events, a control sam-

ple which approximately mimics the features of the  $\tau$  three prongs<sup>18</sup> and which, in principle, has a known mean path length. Comparison between control samples derived from both real and simulated data will provide a measure of how well the Monte Carlo simulation models the tracking system, as well as set an upper limit on the magnitude of any unanticipated form of measurement bias.

The control sample is selected with the following requirements. The events have seven or more charged tracks, sum of scalar momenta for all charged particles between 10 and 30 GeV/c, and overall event vertices that are well measured and near the interaction point. A study of tracking  $\chi^2$  in these events, similar to that described in Sec. III C, indicates that the actual VC resolution is some 30% worse than that for Bhabha tracks. In the same spirit as the discussion of Sec. III C, we therefore refit all tracks with the VC error increased by 30%. We then construct "pseudo- $\tau$ " by selecting from each event the three highest-momentum, well-measured tracks which have a total momentum between 3 and 15 GeV/c, an opening half-angle less than 0.70 rad, and a ratio of total momentum to three-particle invariant mass greater than 4.0. Tracks are not used if, when combined with any oppositely charged track in the event, the two-particle invariant mass is consistent with that of a  $\Lambda^0$  or  $K^0$ .

The control sample constructed from hadronic data is subjected to the  $\tau$  selection procedure and the maximum-likelihood fit for the mean decay length. The result, using the zero-lifetime form, is  $156 \pm 30 \mu\text{m}$ , with  $R = 1.32 \pm 0.05$ .

The same analysis performed on the control sample drawn from simulated hadronic events has a fitted mean path length of  $130 \pm 24 \mu\text{m}$ , with  $R = 1.14 \pm 0.04$ . The magnitude of the finite path length in this sample depends on the values for the  $D^0$  and  $D^\pm$  lifetimes, the  $D^0/D^\pm$  ratio, and the mean  $B$  lifetime. Adding in quadrature the change in the path length resulting from reasonable independent variations in these parameters,<sup>19</sup> we conclude that the total path-length uncertainty expected from these effects is approximately  $12 \mu\text{m}$ .

From this control sample analysis, we make the following observations.

(1) The pseudo- $\tau$  samples from Monte Carlo simulation and data exhibit good agreement, within the errors, in the fitted mean path lengths. We take this agreement as evidence that any potential offset bias in the  $\tau$  analysis is limited by the error in the comparison: namely, the sum in quadrature of the statistical errors and the error from systematic uncertainties in  $D$  and  $B$  lifetime effects. The overall estimated uncertainty is thus  $40 \mu\text{m}$ .

(2) The Monte Carlo pseudo- $\tau$  path-length distribution exhibits a larger width than expected, as characterized by the 14% deviation of the scale factor  $R$  from unity. We have verified that this effect, as well as the finite mean path length, is entirely associated with the presence of heavy-quark decays. It arises from the way in which finite path lengths are generated by the random association of tracks from decays and from the event origin. The distribution of such path lengths is not exponential,

and its rms width is larger than its mean value. The convolution of Sec. IV C is thus not an exact representation, and the fit compensates with an  $R$  value greater than unity.

(3) For pseudo- $\tau$  in real hadron data,  $R$  is found to be 18% higher than for pseudo- $\tau$  in the Monte Carlo distribution. In the case of real  $\tau$  events, the  $R$  value is  $1.05 \pm 0.4$ . This is evidence that the widths of the error distributions in the data are larger than anticipated, and that they are larger in hadronic events than in the relatively cleaner  $\tau$  events. The two parameter fit to  $l_\tau$  and  $R$ , however, leads to a value of  $l_\tau$  which is less sensitive to the exact shape of the resolution function.

#### D. Summary of systematic errors

We find no evidence for significant measurement bias or offset in Monte Carlo study of our analysis procedure. From the comparison of control samples in real and Monte Carlo hadronic events, we assign a systematic uncertainty of  $40 \mu\text{m}$  to such error.

As discussed in Sec. IV E, the presence of backgrounds in the  $\tau$  sample lowers the measured mean decay length by  $31 \pm 10 \mu\text{m}$ .

We check for the presence of other potential biases by repeating the analysis with independent variations of key parameters. Reasonable changes in the  $\sigma_l$  cut, the  $\chi^2$  cut, and other tracking cuts produce no significant variation in  $l_\tau$ . Use of beam positions derived by an alternate method likewise produces no significant change.<sup>14</sup>

The effect of assuming that the three-prong momentum sum exactly follows the  $\tau$  direction is studied via Monte Carlo simulation. The net difference in  $l_\tau$  when the true  $\tau$  direction is substituted for the three-prong momentum sum is found to be  $2 \mu\text{m}$ , and is thus completely negligible.

We conclude that the potential systematic error of this measurement is given by the sum in quadrature of the bias uncertainty and background error, giving a net systematic error of  $41 \mu\text{m}$  in the path length, or  $0.17 \times 10^{-13}$  sec in the lifetime.

## VI. CONCLUSION

We have used a high-resolution vertex detector to measure the lifetime of  $\tau$  leptons produced in electron-positron annihilation at PEP. The result is

$$\tau_\tau = (2.88 \pm 0.16 \pm 0.17) \times 10^{-13} \text{ sec},$$

where the first error is statistical and the second is systematic. This result is consistent with the theoretical prediction, as well as with other recent experimental determinations.<sup>8</sup> Combining in quadrature both experimental errors and the error on the theoretically predicted lifetime, we find that, at 95% confidence, the strength of the  $\tau$  coupling to the charged weak current lies within 9% of the universal Fermi coupling strength.

## ACKNOWLEDGMENTS

This work was supported in part by the Department of Energy, Contracts Nos. DE-AC03-76SF00098 (LBL), DE-AC03-76SF00515 (SLAC), and DE-AC02-76ER03064 (Harvard).

- (a) Present address: University of Chicago, Chicago, IL 60637.
- (b) Present address: Harvard University, Cambridge, MA 02138.
- (c) Present address: Therma-Wave Corp., Fremont, CA 94539.
- (d) Present address: Brookhaven National Laboratory, Upton, NY 11973.
- (e) Present address: California Institute of Technology, Pasadena, CA 91125.
- (f) Present address: Columbia University, New York, NY 10027.
- (g) Present address: University of Illinois, Urbana, IL 61801.
- (h) Present address: LPNHE, Université Pierre et Marie Curie, F-75230 Paris, France.
- (i) Present address: University of California, Santa Cruz, CA 95064.
- (j) Present address: University of Pennsylvania, Philadelphia, PA 19104.
- (k) Present address: CERN, CH-1211, Geneva 23, Switzerland.
- (l) Present address: Oxford University, Oxford, England.
- (m) Present address: University of Geneva, CH-1211 Geneva 4, Switzerland.
- <sup>1</sup>The form of the lowest-order correction to the lifetime is  $1 + 8(m_\nu/m_\tau)^2$ . The effect of a neutrino mass at the experimental upper limit would lengthen the predicted lifetime by 1.2%. See Y. S. Tsai, Phys. Rev. D **4**, 2821 (1971); H. Albrecht *et al.*, Phys. Lett. **163B**, 404 (1985).
- <sup>2</sup>A. Sirlin, Phys. Rev. D **22**, 971 (1980).
- <sup>3</sup>P. R. Burchat, in *Proceedings of the XXIII International Conference on High Energy Physics*, Berkeley, California, 1986, edited by S. C. Loken (World Scientific, Singapore, 1987).
- <sup>4</sup>Particle Data Group, M. Aguilar-Benitez *et al.*, Phys. Lett. **170B**, 1 (1986).
- <sup>5</sup>A. De Rújula, in *Weak and Electromagnetic Interactions at High Energy*, 1976 Les Houches Lectures, edited by R. Balian and C. H. Llewellyn Smith (North-Holland, Amsterdam, 1977).
- <sup>6</sup>M. Gronau, C. N. Leung, and J. L. Rosener, Phys. Rev. D **29**, 2539 (1984); X. Y. Lee and E. Ma, Phys. Rev. Lett. **47**, 1788 (1981); L. Abbott and E. Farhi, Phys. Lett. **101B**, 69 (1981).
- <sup>7</sup>D. A. Bryman *et al.*, Phys. Rev. Lett. **50**, 7 (1983).
- <sup>8</sup>H. R. Band *et al.*, Phys. Rev. Lett. **59**, 415 (1987); C. Bebek *et al.*, Phys. Rev. D **36**, 690 (1987); S. Abachi *et al.*, Phys. Rev. Lett. **59**, 2519 (1987).
- <sup>9</sup>J. A. Jaros, in *The Sixth Quark*, proceedings of the 12th SLAC Summer Institute on Particle Physics, Stanford, California, 1984, edited by P. McDonough (SLAC Report No. 281, Stanford, 1985); J. A. Jaros *et al.*, Phys. Rev. Lett. **51**, 955 (1983).
- <sup>10</sup>R. H. Schindler *et al.*, Phys. Rev. D **24**, 78 (1981).
- <sup>11</sup>R. H. Schindler, Ph.D. thesis, Stanford University, SLAC Report No. 219, 1979.
- <sup>12</sup>J. Jaros, in *Proceedings of the International Conference on Instrumentation for Colliding Beam Physics*, Stanford, California, 1984, edited by W. W. Ash (SLAC Report No. 250, Stanford, 1982).
- <sup>13</sup>M. Atac, IEEE Trans. Nucl. Sci. **31**, 99 (1984).
- <sup>14</sup>L. Gladney *et al.*, Phys. Rev. D **34**, 2601 (1986).
- <sup>15</sup>The final values for the beam sizes derived from the full data set are  $\sigma_{bx} = 423 \pm 14 \mu\text{m}$  and  $\sigma_{by} = 72 \pm 9 \mu\text{m}$ . The small change from the values in Sec. II C has no effect on the measured mean path length. See Ong (Ref. 17).
- <sup>16</sup>P. R. Burchat *et al.*, Phys. Rev. Lett. **54**, 2477 (1985); B. G. Bylsma *et al.*, Phys. Rev. D **35**, 2269 (1987).
- <sup>17</sup>Rene Ong, Ph.D. thesis, Stanford University, SLAC Report No. 320, 1987.
- <sup>18</sup>The momenta of the hadronic three-prong combinations are smaller than those of  $\tau$ , and the hadronic tracking environment is more crowded.
- <sup>19</sup>J. C. Anjos *et al.*, Phys. Rev. Lett. **58**, 311 (1987); M. G. Gilchriese, in *Proceedings of the XXIII International Conference on High Energy Physics* (Ref. 3); Berkeley, California, edited by S. C. Loken (World Scientific, Singapore, 1987); M. Derrick *et al.*, Phys. Rev. Lett. **53**, 1971 (1984).